AIAA JOURNAL
Vol. 44, No. 10, October 2006

Stochastic Nonparametric Models of Uncertain Hysteretic Oscillators

S. F. Masri,* R. Ghanem,† F. Arrate,‡ and J. P. Caffrey§
University of Southern California, Los Angeles, California 90089-2531

DOI: 10.2514/1.19859

A study is presented of the significant issues encountered in the modeling and characterization of uncertainties in the parameters of hysteretic nonlinear systems that are subjected to deterministic excitations. A single-degree-of-freedom system, with bilinear hysteretic characteristics, is employed to investigate the propagation of uncertainties in the dominant parameters that control the idealized restoring force associated with such a system. Random variations are introduced in the nominal value of each of the dominant parameters. Monte Carlo simulation approaches are used to generate a large, statistically significant, ensemble of time history records that are subsequently used to determine the distribution of the corresponding transient response and establish the probabilistic bounds on the response time history. The restoring force method is used to determine the power-series coefficients that define an approximating surface that characterizes the system behavior. The statistics of the identified coefficients are determined and shown to provide a powerful tool for quantifying the level and features of the uncertainty in the nonlinear system. Furthermore, it is shown that the general methodology presented allows the estimation through analytical procedures of the uncertain system's response bounds when it is excited by a different dynamic load than the one used to identify it.

Nomenclature

a_{ij}	=	denormalized power-series coefficients
C_{ij}	=	Chebychev series coefficients
CV	=	coefficient of variation; σ/μ
c_1	=	bilinear hysteretic element viscous damping coefficient in the linear range
c_2	=	bilinear hysteretic element viscous damping coefficient in the yielded range
$f(t)$	=	applied force
k_1	=	bilinear hysteretic element stiffness in the linear range
k_2	=	bilinear hysteretic element stiffness in the yielded range
m	=	system mass
r	=	exact restoring force
$\hat{r}(x, \dot{x})$	=	estimated restoring force
T_k	=	Chebychev polynomial of order k
x	=	displacement
x_y	=	bilinear hysteretic element yield level
μ	=	mean
$\{\psi_p(\theta)\}$	=	set of orthogonal random variables used in the decomposition of $C(\theta)$
σ	=	standard deviation
θ	=	random parameter
$(\bullet)'$	=	denotes normalization in the range ± 1.0

Received 2 September 2005; revision received 5 March 2006; accepted for publication 6 March 2006.

*Professor in Civil Engineering, School of Engineering, 210 Kaprielian Hall; masri@usc.edu. Member AIAA.

†Professor in Civil Engineering, School of Engineering, 210 Kaprielian Hall; ghanem@usc.edu.

‡Research Assistant in Civil Engineering, School of Engineering, 210 Kaprielian Hall.

§Research Assistant Professor in Civil Engineering, School of Engineering, 210 Kaprielian Hall.

I. Introduction

In spite of the tremendous strides being continuously made in the processing capabilities of digital computers, there is still a need for a capability to perform *accurate*, simulated experiments on realistic complex nonlinear systems in either existing or conceptual design stages. With the current state-of-the-art computational tools for nonlinear systems, users are usually able to obtain results that are satisfactory for estimating the gross behavior of nonlinear systems, but are inaccurate in representing the fine details of such systems, due to the wrong physics that is incorporated in the simulation model. A formidable hurdle preventing the use of sophisticated computational tools replicating the behavior of existing physical structures or simulating the response of complex nonlinear systems in the design stage, is the lack of high-fidelity, physics-based, robust nonlinear computational models that accurately reflect the multidimensional behavior of such systems under arbitrary dynamic environments.

Related issues that are crucial to the development of useful computational models (which, for example, can be relied on to reduce the number of physical tests needed for certification of actual physical systems), on the basis of measurements obtained from nonlinear physical models, are 1) the quantification of uncertainties that are inherently present in the underlying physical prototype, 2) the determination of the corresponding uncertainties in the identified reduced-order, reduced-complexity mathematical model, and 3) the subsequent quantification of the propagation effects of these physical uncertainties in the identified model, as well as the uncertainty bounds on the dynamic system response.

The results of a comprehensive computational study focused on a subset of the issues needed to resolve some of the daunting problems that hinder the development of reliable general-purpose computer simulation programs are reported in this paper. Such computational tools would be capable of reflecting precisely the dynamic behavior of distributed, nonlinear systems spanning the range from large joint-dominated space structures, to intricate electromechanical systems, to microelectromechanical systems, as well as civil infrastructure systems.

For predictive models to fulfill their potential as surrogates to physical experiments, and therefore be reliable tools for analytical certification, they should be capable of capturing the salient features of these experiments. In particular, the variability generally observed in experimental data incorporates uncertainties in the behavior of the associated system, hence the need for stochastic predictive models. A number of issues are associated with such models. One important

issue is the need for the development of a measure of closeness between model-based predictions and experimental data that reflects the statistical content of information as well as the mechanics of the problem. In addition, methods for controlling this measure, either through model refinement or through statistical and data refinement, must be available. The problem, therefore, can be characterized as a problem of error estimation and control in a statistical environment. A mathematical framework that makes the required connection between statistical estimation and approximation theory has been developed by one of the authors, and can be used to both quantify and manage the uncertainty in model-based predictions. Once the uncertainty in model predictions is consistent with the experimental uncertainty, the model can be classified as validated, and its use in analytical certification is justified.

Further background information regarding the approaches and challenges in the representation and propagation of uncertainties in structural systems is available in the works of Ghanem [1], Ibrahim [2], Ibrahim and Pettit [3], Lin and Cai [4], Pettit [5], Pellissetti and Ghanem [6], Sakamoto and Ghanem [7,8], Soize and Ghanem [9], and Spanos and Ghanem [10].

With the ever-increasing cost of experimental tests of complex structural systems that may incorporate nonlinear (i.e., not necessarily linear) elements, there is an increasing interest in developing sophisticated computational tools that employ high-fidelity mathematical models that can be used to mimic the behavior of systems (existing structures or those in the conceptual design stage) under arbitrary dynamic environments. Although there is no shortage of available computer codes that have extensive libraries of elements and which can model a broad array of nonlinear phenomena with virtually no restriction on the number of elements, these codes are limited in their range of validity to reproduce only nonlinear behavior which is already modeled in their element library. In other words, the accuracy of all available computer codes to estimate the dynamic response of complex systems is only as good as the accuracy of the physics that underpins the elements incorporated in the assembled mathematical model whose motion is to be simulated. The lack of appreciation of this basic, but obvious, fact has resulted in the use of ever more complex mathematical modeling with the available computational tools yielding more precise but erroneous answers, due to the wrong physics that is embodied in the simulation model.

In view of the need for computational tools that provide accurate simulation results for situations requiring high resolution in representing the detailed behavior of nonlinear systems, there is a demand for physics-based, high-fidelity, reduced-order, nonlinear mathematical models that can serve as the underpinnings of reliable software tools to perform accurate simulation studies of intricate nonlinear systems, spanning the range from large joint-dominated space structures, to electromechanical systems, to adaptive (nonlinear) materials, to microelectromechanical systems, as well as to civil infrastructure systems.

The work reported in this paper is focused on developing methods and procedures suitable for use with structural response measurements from flexible structural components and assemblages that may incorporate elements undergoing significant nonlinear behavior. The aim is to evaluate the usefulness of suitable reduced-order mathematical models characterizing the essential features of the dominant structural behavior. Such models can serve a dual purpose: as an efficient tool for analysts who need to predict the behavior of similar structures under dynamic loads, as well as being a useful tool for condition assessment and damage detection (Housner et al. [11]).

The vast majority of system identification procedures available today are based on the assumption that the structure will behave in a linear fashion. The state-of-the-art linear system identification approaches have advanced to such an extent that commercial software packages are currently available for online identification of such linear properties as natural frequencies, mode shapes, and damping ratios. However, the scope of available approaches for identification of nonlinear structural behavior is much more limited. The common approach based on Volterra integrals is, generally, unsuitable for practical application due to excessive data storage and computation requirements, as well as restrictions on the nature of excitation and class of nonlinearities to be identified.

A restricted class of nonlinear identification procedures is based on parametric methods, where all degrees of freedom are included in the model, and nonlinearities are modeled in detail, with only their parameters to be identified (Wen [12], Andronikou et al. [13], Worden [14], Chassiakos et al. [15], Banks et al. [16–18], Smyth et al. [19,20]). Then, a standard least-squares fit, in the time or frequency domain, may be used to identify the parameters. Such an approach is not advisable for actual structures incorporating complex nonlinearities, because the number of parameters to be identified would be prohibitive, and, in addition, the nature of the nonlinearity may not be adequately known a priori to construct a representative parametric model.

An alternative approach for the identification of nonlinear systems is the nonparametric approach that is based on the restoring force method (Masri and Caughey [21]) that develops an approximating analytical function to represent the restoring force surface associated with the nonlinear system being analyzed. To obtain the coefficients involved in the series representation of the restoring force, a nonlinear regression in the time domain is performed. The object of this regression is to identify the coefficients in a power-series representation of the restoring force onto the acceleration, velocity, and displacement. The order of the power series is not predetermined, but is obtained recursively during the identification. In the case of multi-degree-of-freedom systems, the power series is, of course, multidimensional and allows for modal interaction effects between the displacements, velocities, and accelerations associated with different basis vectors. The end result is a set of truncated power series with known coefficients and a set of coordinate transformations that may be used to completely define the dynamics of the original system to arbitrary excitations (Masri et al. [22]).

Although the assumed representation for the restoring forces may at first appear restrictive, results in applications have shown that the restoring force method (RFM) may be applied with confidence to problems involving not only deadspace and Coulomb friction nonlinearities, but also to problems involving structural hysteresis. The results, even for hysteretic systems (which are known to admit no analytic representation), are excellent in both the time domain and frequency domain.

Over the years, the RFM has been successfully applied to synthetic and experimental data obtained during a wide variety of conditions ranging from earthquake response of large buildings (Anderson et al. [23]), to laboratory tests of frictional bearings (Masri et al. [24]), to nonlinear dampers (Worden and Tomlinson [25]), and to complex nonlinear systems such as the Duffing–van der Pol oscillator (Masri et al. [22,26]).

In Sec. II, an overview of the modeling and nonparametric identification procedure and its application to the identification of the transient response of a bilinear hysteretic oscillator with uncertain parameters under swept-sine excitation is presented. The sensitivity of the hysteretic system response to perturbation in three dominant model parameters is determined, and their effects as propagated through the restoring force coefficients are quantified. A discussion is presented in Sec. III concerning the significance of the simulation results and their implication in planning an adequate procedure to quantify and represent the effects of uncertainties on the transient response of complex nonlinear systems.

II. Uncertain Hysteretic System Under Swept-Sine Excitation

A. State Equations for Complex Nonlinear Systems

To demonstrate how the general method under discussion can be adapted to deal with a subset of complex nonlinear systems, consider a single degree of freedom whose motion is governed by

$$m\ddot{x} + r(x, \dot{x}, \boldsymbol{p}) = f(t) \tag{1}$$

where $\ddot{x}$ is the system acceleration and $\boldsymbol{p}$ is a parameter vector that characterizes the system nonlinearity. This equation governs a very

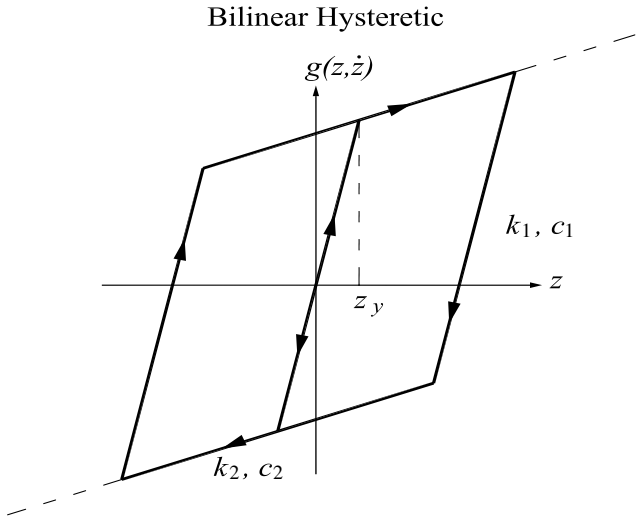

$p_1 = z_y$ = yield displacement level
$p_2 = k_1$ = stiffness in elastic range
$p_3 = k_2$ = stiffness in nonlinear range
$p_4 = c_1$ = viscous damping term in elastic range
$p_5 = c_2$ = viscous damping term in nonlinear range

Fig. 1 Control parameters p that define the force-deformation characteristics of the damped bilinear hysteretic oscillator.

broad class of hysteretic systems spanning the range from a completely elastic to a completely elastoplastic hysteretic oscillator, specified by parameters $\boldsymbol{p}$, under exciting force $f(t)$. Note also that the general formulation of Eq. (1) applies as well to systems with arbitrary nonlinear restoring forces such as those involving Coulomb friction, deadspace, saturation, limited-slip, etc.

B. Response of Reference Bilinear Hysteretic Oscillator Under Swept-Sine Excitation

The bilinear hysteretic (BLH) element is characterized by the following parameters: $\boldsymbol{p}_1 = x_y$ is the yield level, $\boldsymbol{p}_2 = k_1$ is stiffness in the linear range, $\boldsymbol{p}_3 = k_2$ is stiffness in the yielded range, $\boldsymbol{p}_4 = c_1$ is viscous damping coefficient in the linear range, and $\boldsymbol{p}_5 = c_2$ is viscous damping coefficient in the yielded range. The idealized force-deformation characteristics of the damped bilinear hysteretic oscillator are shown in Fig. 1. The illustrative example used here had the following system parameters: $x_y = 0.02$, $k_1 = 1.0k_0$, $k_2 = 0.10k_0$, $c_1 = 0.01$, and $c_2 = 0.01$, with $m = 1.0$ and $k_0 = (2\pi)^2$.

The example hysteretic system under discussion was subjected to a swept-sine excitation of amplitude $f_0 = 0.02k_0$ applied for a duration of $t_{\max} = 5.0T_0$, with a lower frequency $\omega_{\text{lower}} = 0.90\omega_n$, and $\omega_{\text{upper}} = 1.10\omega_n$ changing linearly over a period of $10T_0$, where T_0 was selected as equal to 1.0, and $\omega_n = 2\pi$. The time history of the excitation $f(t)$ as well as the resulting reference system response are shown in Fig. 2, where Fig. 2a shows the time history of the excitation, Fig. 2b the corresponding time history of the restoring force $r(t)$, Fig. 2c a phase diagram of the system velocity vs. the corresponding displacement, and Fig. 2d the phase diagram of the restoring force vs. the corresponding displacement.

C. Uncertain Hysteretic System Parameters Under Swept-Sine Excitation

To investigate the sensitivity of the hysteretic oscillator under discussion to uncertainties in its parameters, four cases were simulated and are summarized in Table 1.

Each of the cases listed in Table 1 involved conducting a Monte Carlo simulation in which the indicated BLH parameter was randomly varied according to a truncated Gaussian distribution, in which the lower values were constrained not to be less than 1% of the respective mean. This was accomplished by rejecting randomized values of the uncertain parameters that fell outside their respective bounds.

For case 1, the 2000 random values of the randomized parameter x_y that governs the yield range (Fig. 1), are plotted in the upper left-hand-side (LHS) column of Fig. 3. In this figure, the abscissa corresponds to the index i of simulation cases, and the ordinate shows the corresponding uncertain value of x_y for each of the simulation cases. Note that the random values of x_y hover around the mean value $x_{y,\text{mean}} = 0.02$ selected for this demonstration case.

The middle column of plots in Fig. 3 shows the corresponding histogram and a superposed Gaussian probability density function (PDF) having the same mean and variance of the ensemble. The right-hand-side (RHS) column of plots in Fig. 3 shows a plot of the distribution of the uncertain values of the investigated parameters when plotted on Gaussian paper on which a random variable that is truly Gaussian in nature will generate a straight line plot. The histogram plot in the middle column of plots shows a skewed distribution in the first bin (the lower bound) of the distribution. This is caused by the fact mentioned previously that, to preserve realism in the selection of the uncertain system parameters, their minimum

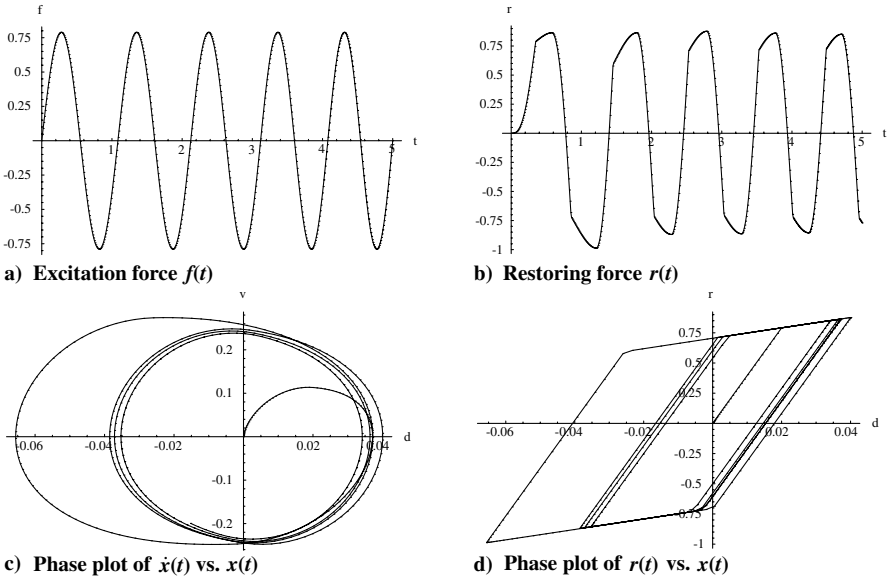

a) Excitation force $f(t)$ b) Restoring force $r(t)$

c) Phase plot of $\dot{x}(t)$ vs. $x(t)$ d) Phase plot of $r(t)$ vs. $x(t)$

Fig. 2 Swept-sine excitation and response of reference hysteretic system.

Table 1 Summary of simulation cases performed with an uncertain system under swept-sine excitation

Case number	Case specifications; ($CV = \sigma/\mu$)
1	Swept-sine excitation; $CV_{x_y} = 0.50$
2	Swept-sine excitation; $CV_{k_1} = 0.50$
3	Swept-sine excitation; $CV_{k_2} = 0.50$
4	Swept-sine excitation; $CV_{x_y} = CV_{k_1} = CV_{k_2} = 0.50$

value was constrained to be $\geq 1\%$ of the corresponding mean. Careful inspection of the plots in the RHS column shows that the plotted variables do indeed follow a straight line form, except at the extreme (lower) range of the random variable magnitude.

In case 2, an ensemble of 2000 cases is generated in which all the BLH system parameters are kept the same as the nominal case, except that for k_1 the stiffness in the linear range is randomly varied according to a clipped Gaussian distribution in which the lower values are constrained to be $\geq 1\%$ of the respective mean. The corresponding results are shown in the middle row of Fig. 3. Note that the random values of k_1 hover around the mean value of $k_{1,\text{mean}} \approx 40.0$.

Similarly, in case 3, an ensemble of 2000 cases is generated in which all the BLH system parameters are kept the same as the nominal case, except that for k_2 the stiffness in the nonlinear range is randomly varied according to a clipped Gaussian distribution in which the lower values were constrained to be $\geq 1\%$ of the respective mean. The corresponding results are shown in the bottom row of Fig. 3. Note that the random values of k_2 hover around the mean value of $k_{2,\text{mean}} \approx 4.0$.

It is worth noting from the middle column of histograms plotted in Fig. 3 that, even with just 2000 simulations, the results closely match an ideal Gaussian PDF. Had more ensembles been generated, a smoother-looking histogram would have resulted. Also, notice that, to maintain physical realism in the range of randomized hysteretic oscillator parameters, there are no negative values obtained for the uncertain parameters.

The LHS column of the plots in Fig. 4 shows the scatter diagram for the hysteretic system rms displacement response, the middle column of plots shows the corresponding sorted values of the LHS column, and the RHS column of plots displays the same results on probability paper. The PDF of the displacement rms for the four simulation cases is shown in Fig. 5.

D. Sensitivity of Hysteretic System Response Under Swept-Sine Excitation to Uncertain Parameters

The resulting mean $E[r(t)]$ and standard deviation $\sigma_r(t)$ of the restoring force ensemble $\langle r(t) \rangle$ for four simulation cases under investigation (Table 1) are depicted in Fig. 6 first row, case 1; second row, case 2; third row, case 3; fourth row, case #4. For all the plots, the mean is shown by a solid line and the corresponding standard deviation by a dotted line.

It is clear from inspection of the plots shown in Fig. 6 that the transient response of the hysteretic oscillator has different sensitivities to the three control parameters investigated herein: x_y, k_1, and k_2. This variation in sensitivity is easier to discern from the results shown in Fig. 7. The plot in the top row of the LHS column in Fig. 7a shows the mean of the restoring force $E[r(t)]$ for the system response corresponding to cases 1, 2, and 3 (solid line, small-dash line, and long-dash line, respectively). The corresponding standard deviation of the system restoring force $\sigma_r(t)$ for the same three simulation cases are shown in the RHS column of Fig. 7b. The plots shown in the lower row of Fig. 7 correspond to the displacement response mean $E[x(t)]$ (in Fig. 7c) and response standard deviation $\sigma_x(t)$ [in Fig. 7d].

Analysis of the results shown in Fig. 7 indicates that the variance of the transient response of the hysteretic system is most sensitive to large variations in the stiffness in the linear range k_1, next in sensitivity is the variance due to randomness in the yield level x_y, and least in sensitivity is the stiffness in the nonlinear range k_2. The variance in the system restoring force is about a factor of two higher in frequency, as compared with the corresponding variance in the system displacement response. Although the variation in the mean value of the restoring force or the displacement is quite small when compared with the three test cases, there are substantial differences in the level, as well as in the spectral content of the evolving standard deviation, of both the restoring force and the system displacement.

It is seen that a 50% variation in the mean value of x_y, k_1, and k_2, whereby each indicated parameter is made uncertain one at a time, results in a standard deviation of $r(t)$ whose peak is about 1.0, 1.4, and 0.2 times the corresponding levels of standard deviations $\sigma_{x_y} = 0.5$, $\sigma_{k_1} = 0.5$, and $\sigma_{k_2} = 0.5$, respectively. Similarly, in the case of uncertainty of the same levels, the standard deviation peak in the system displacement response yields standard deviation peak levels that are about 0.85 σ_{x_y}, 0.95 σ_{k_1}, and 0.25 σ_{k_2} times the corresponding levels of standard deviations.

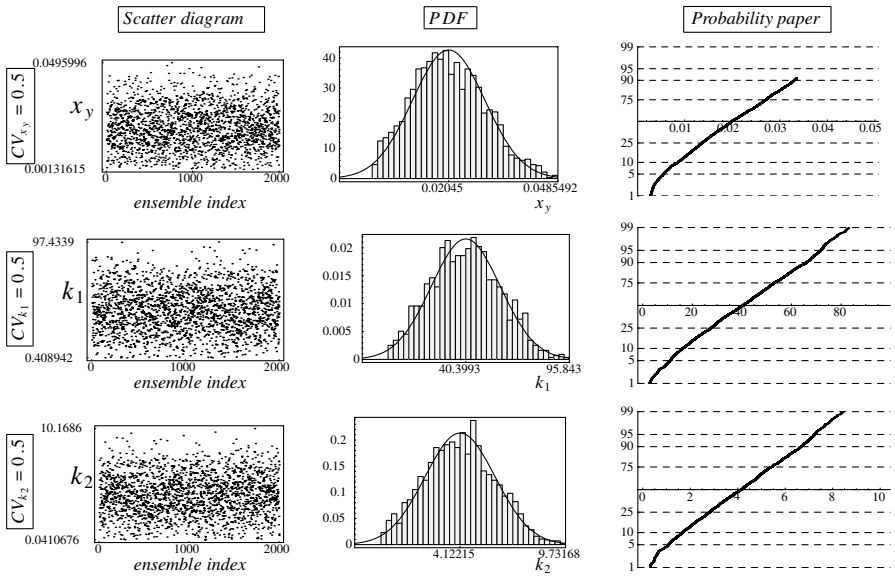

Fig. 3 Statistical characteristics of x_y, k_1, and k_2 under swept-sine excitation. The first (top) row of plots corresponds to statistics of x_y; the second row shows the k_1 statistics; and the third row shows the k_2 statistics. The LHS column shows the scatter diagrams of each of the uncertain parameters plotted as a function of the simulation case index number i; the middle column shows the corresponding histogram and a superposed Gaussian PDF; the RHS column shows a plot of each random parameter on probability paper whereby a truly Gaussian distribution would yield a straight line.

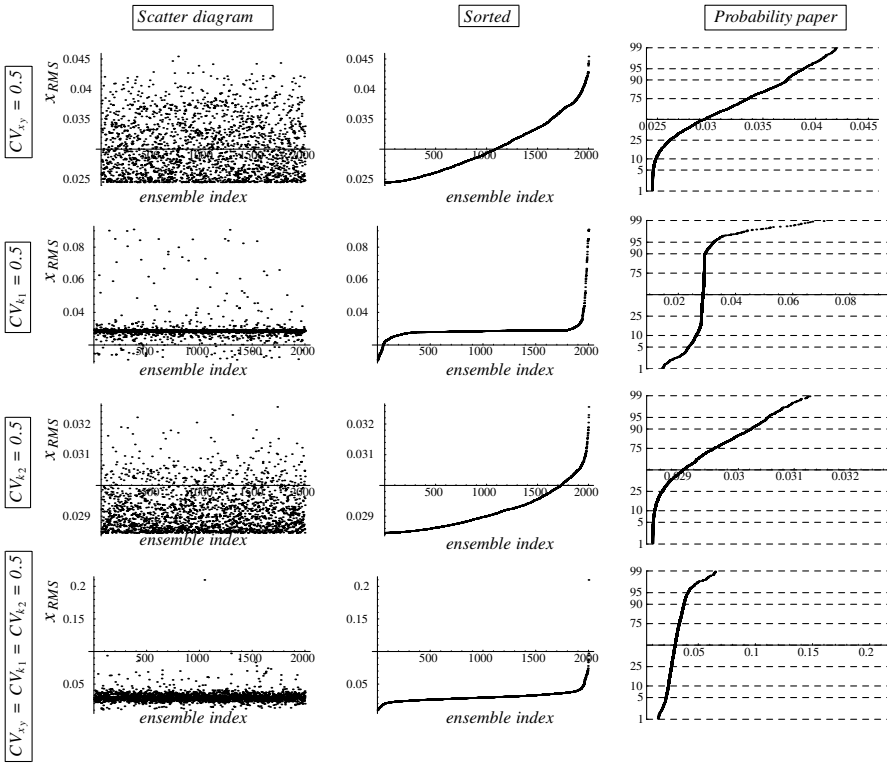

Fig. 4 Scatter diagrams and probability paper plots of displacement rms distribution for four simulation cases. The top row corresponds to uncertainty only in x_y; the second-from-top row corresponds to uncertainty only in k_1; the third-from-top row corresponds to uncertainty only in k_2; and the bottom row corresponds to uncertainty simultaneously in x_y, k_1, and k_2.

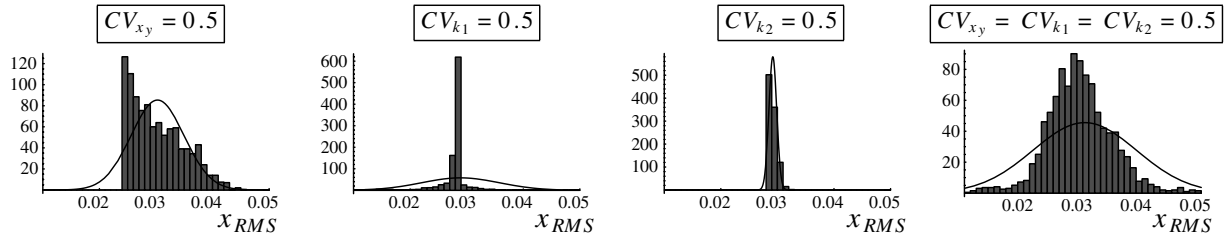

a) Uncertainty only in x_y

b) Uncertainty only in k_1

c) Uncertainty only in k_2

d) Uncertainty simultaneously in x_y, k_1, and k_2

Fig. 5 PDF of displacement rms distribution for four simulation cases.

To help interpreting the significance and implications of the results displayed in Fig. 7, it is useful to plot the transient time history of the restoring force, as well as the system displacement, with an uncertainty band corresponding to a range of $\pm 1.0\sigma$ with respect to the corresponding ensemble mean. This is accomplished in Fig. 8, in which the LHS column of plots shows four panels of plots. In each panel, three curves are shown: the solid line corresponds to the mean of the restoring force $E[r(t)]$, the small-dash line shows the mean plus 1.0σ bound $(E[r(t)] + \sigma_r)$, and the large-dash line shows the mean minus 1.0σ bound $(E[r(t)] - \sigma_r)$. Similar results are shown in the RHS column of the plots in Fig. 8 for the system displacement.

Inspection of the plots in Fig. 8 shows that the type of parameter uncertainty manifests itself in the system restoring force and displacement in a time-varying, complex, nonlinear fashion. Note from the bottom row in Fig. 8 that when simultaneous, uncorrelated uncertainties (each having a standard deviation of 50% around the mean of the corresponding parameter) are introduced in the three controlling parameters, the uncertainty band in the system response is not just the additive sum of the individual contributions, due obviously to the complex phase effects in how the uncertainties are propagated in the nonlinear system response.

E. Identification of Restoring Force Coefficients for Reference Case

The central idea of the restoring force method (Masri and Caughey [21]) is that, in the case of nonlinear dynamic systems commonly encountered in the structural mechanics field, a judicious assumption is that the restoring force r can be expressed in terms of a series of the form

$$r \approx \hat{r}(x, \dot{x}) \equiv \sum_{i=0}^{i_{\max}} \sum_{j=0}^{j_{\max}} C_{ij} T_i(x') T_j(\dot{x}') \tag{2}$$

The series appearing in Eq. (2) can be converted to a power series of the form

$$\hat{r}(x, \dot{x}) \equiv \sum_{i=0}^{i_{\max}} \sum_{j=0}^{j_{\max}} a_{ij} x^i \dot{x}^j \tag{3}$$

Application of the nonparametric identification approach to the measurements from the reference hysteretic system discussed previously yields the identification results summarized in Tables 2–4. Thus, at the conclusion of the identification task, the dominant features of the test article are embedded in the normalized Chebychev

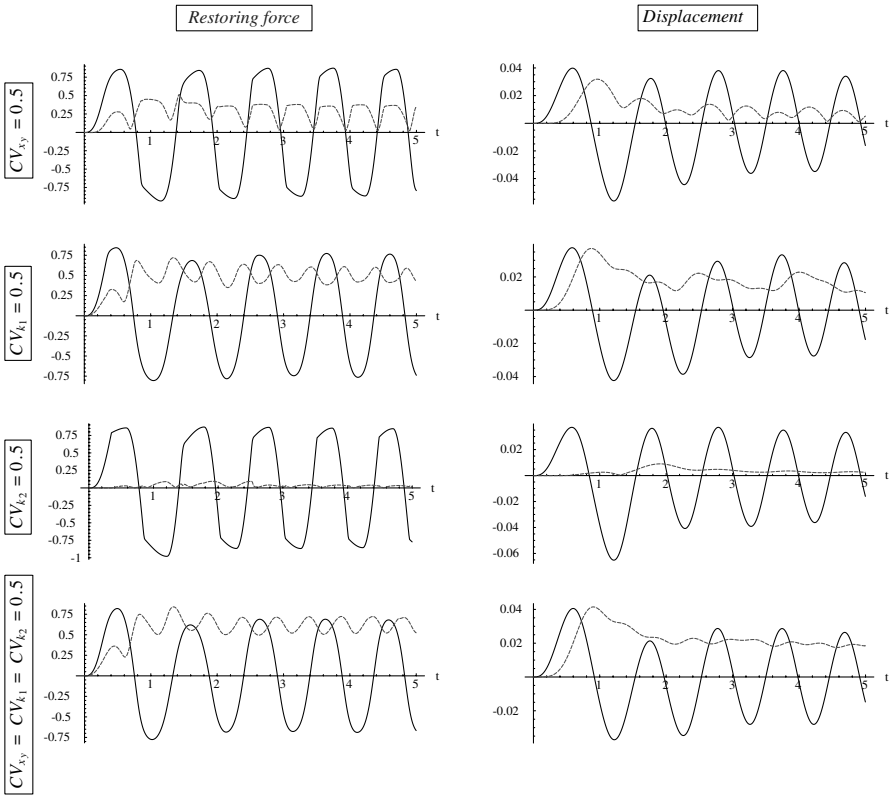

Fig. 6 Time histories of the BLH system ensemble with mean and standard deviation. The LHS column is the restoring force $E[r(t)]$ and $\sigma_r(t)$, and the RHS column is the displacement $E[x(t)]$ and $\sigma_x(t)$. The top (first) row of columns corresponds to the perturbation effects of x_y; the second row, to the effects of perturbing k_1; the third row, to the effects of perturbing k_2; and the fourth (bottom) row shows the effects of simultaneously perturbing all the three indicated variables. In each plot panel, the solid line corresponds to the mean, and the dashed line to the corresponding standard deviation.

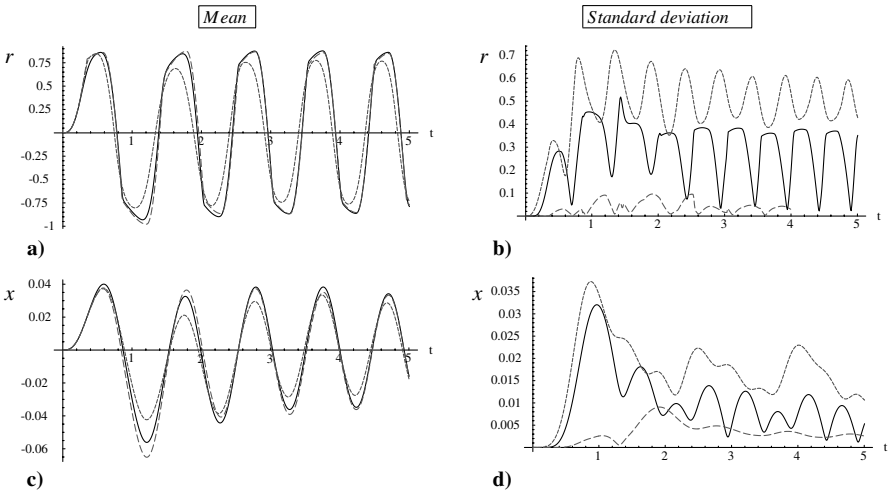

Fig. 7 Time histories of the BLH system ensemble with mean and standard deviation. The LHS column is the mean restoring force and mean displacement; the RHS column is the standard deviation of the restoring force and displacement. In each panel, the solid line is for variation in x_y, the small-dash line is for variation in k_1, and the large-dash line is for variation in k_2.

series coefficients C_{ij} or the denormalized power-series coefficients a_{ij}.

It is seen from the results in Table 4 corresponding to the denormalized power-series coefficients that term a_{10} corresponding to the equivalent linear stiffness term has a value of about 29, which is between the value of k_1 chosen as $(2\pi)^2 \approx 40$ and k_2 whose value is chosen equal to ≈ 4, but much closer to the value of k_1 because the motion of the hysteretic oscillator is primarily in the linear range. Similarly, term a_{01}, corresponding to the equivalent viscous damping term, has a value of about 0.82. The fact that the system has a softening stiffness characteristic when it reaches the yield level is reflected in the value of the coefficient of the nonlinear (cubic) stiffness term whose coefficient a_{30} is equal to -3542.

Using the normalized coefficients shown in Table 3, the relative contribution of the cubic-stiffness term as compared with the equivalent linear stiffness term is given by the ratio of $a_{30}/a_{10} = 0.547/1.490 \approx 0.37$, and the sign associated with the nonlinear stiffness term is negative, indicating a softening contribution. Similarly, it can be inferred from the same table that the contribution of the peak equivalent viscous damping force as compared with the linear stiffness force is given by the ratio $a_{01}/a_{10} = 0.124/1.490 \approx 0.08$.

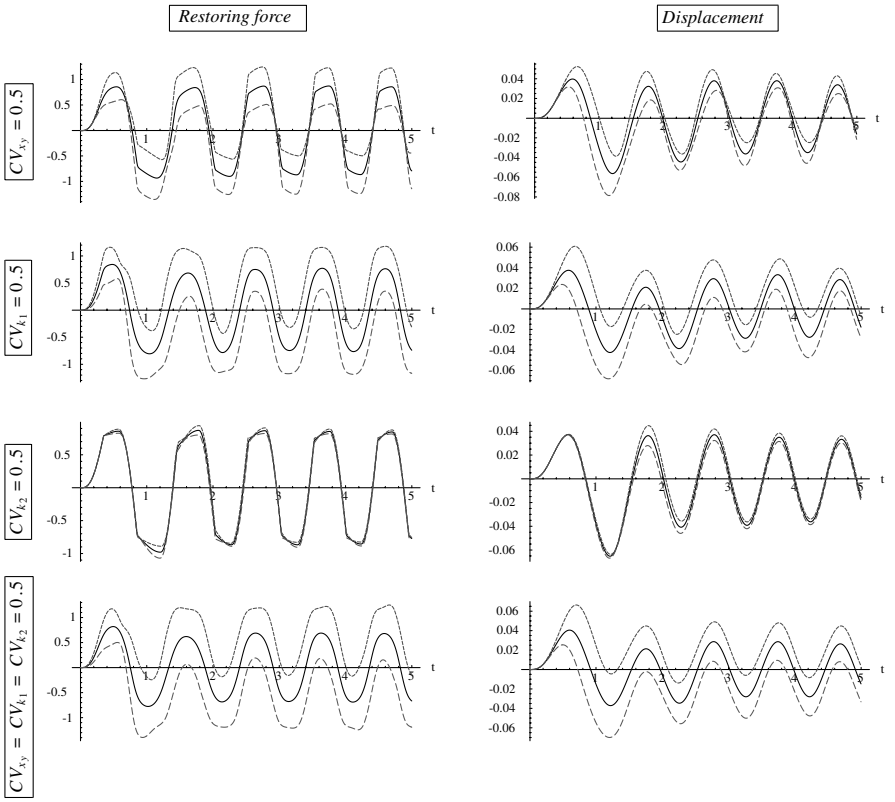

Fig. 8 Time histories of the BLH system ensemble mean and $\pm 1.0\sigma$ bounds. The LHS column depicts the restoring force; the RHS column, the displacement. Each row corresponds to one of the test cases listed in Table 1. The solid line is the mean; the upper bound (small dash) is the mean $+\sigma$; the lower bound (large dash) is the mean $-\sigma$.

The accuracy of the fit between the identified restoring force and the reference restoring force is shown in Fig. 9, in which the solid line represents the exact $r(t)$, whereas the broken line represents the estimated $\hat{r}(t)$. The normalized mean square error of the deviation between the two records in this case is equal to 0.084, that is, it is 8.4%.

Table 2 Identified restoring force surface coefficients for a reference case under swept-sine excitation; Chebychev coefficients C_{ij}

	$T_0(\dot{x}')$	$T_1(\dot{x}')$	$T_2(\dot{x}')$	$T_3(\dot{x}')$
$T_0(x')$	−0.020	0.399	0.185	0.080
$T_1(x')$	0.785	−0.159	−0.292	−0.060
$T_2(x')$	0.241	−0.168	0.082	−0.067
$T_3(x')$	−0.136	−0.095	0.001	0.011

Table 3 Normalized power-series coefficients a_{ij}

	$\dot{x}'^0$	$\dot{x}'^1$	$\dot{x}'^2$	$\dot{x}'^3$
x'^0	−0.36	0.12	0.21	0.59
x'^1	1.49	0.40	−0.59	−0.37
x'^2	0.32	0.07	0.33	0.54
x'^3	−0.55	−0.51	0.01	0.17

Table 4 Denormalized power-series coefficients a_{ij}

	$\dot{x}^0$	$\dot{x}^1$	$\dot{x}^2$	$\dot{x}^3$
x^0	0.00	0.817	0.21	26.5
x^1	28.9	27.9	−94.2	−636
x^2	−22.4	−460	2064	−8369
x^3	−3542	−13181	−2047	65022

F. Statistical Characteristics of Uncertain Restoring Force Coefficients Under Swept-Sine Excitation

An ensemble of 2000 cases corresponding to each of the three cases is shown in Fig. 3, in which one bilinear hysteretic system parameter was randomized, whereas the remaining ones were kept equal to their reference values. Additionally, as summarized in Table 1, one more simulation case was conducted in which the three parameters x_y, k_1, and k_2 were simultaneously randomized so as to have a Gaussian distribution with a mean equal to the reference value listed previously, and each parameter having a standard deviation of 0.5 of the corresponding mean (i.e., having a $CV = 0.5$).

The nonparametric identification procedure discussed previously was applied to each member of the individual data sets of the large ensemble of tests. The corresponding histogram plots for the normalized errors corresponding to the four cases listed in Table 1 are plotted in Fig. 10. For ease of comparison, identical abscissa scales are used for all cases. Because the value of the normalized error ϵ is a direct measure of the accuracy of the fit (hence, a quantitative measure of the modeling error for each identified case), it is obvious that excellent fidelity is achieved for all the four identification cases, with the mean value of ϵ hovering around 10%.

The plots shown in Fig. 11 provide a summary of the statistical behavior of three of the dominant coefficients that define the restoring force surface: a_{10}, a_{01}, and a_{30}. These specific terms among the 16 coefficients that characterize the surface (if a third-order Chebychev fit is selected for the identification task), do have a physical interpretation associated with them; namely, the equivalent linear stiffness coefficient, the equivalent linear viscous damping term, and the magnitude that scales the cubic-stiffness term, respectively.

The LHS column of the plots in Fig. 11 corresponds to the a_{10} histogram, the middle column to the a_{01} histogram, and the RHS column to the a_{30} histogram. The first (top) row of histograms in Fig. 11 corresponds to case 1 in which parameter x_y was the only one perturbed relative to its reference case; the second row from the top, to case 2 in which only k_1 was randomized; the third row from the top,

to case #3 in which only k_2 was randomized; and the bottom row, to case #4 in which all three parameters x_y, k_1, and k_2 were simultaneously, and independently, randomized with respect to their reference values. For ease of comparison, identical abscissa plot ranges are used for each plot column (i.e., for the same power-series coefficient).

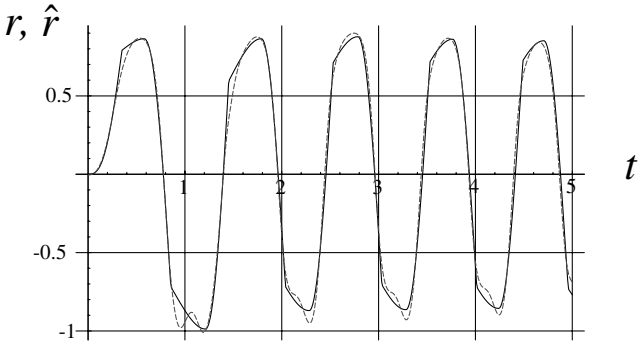

Fig. 9 Comparison between exact and estimated restoring force $r(t)$.

It is clear from inspection of the results depicted in Fig. 11 that, in general, the distribution governing the probability density function for the identified coefficients is far from being Gaussian. Furthermore, depending on the nature of the specific randomized parameter, the variations in a specific parameter manifest themselves in a complex nonlinear way in the corresponding identification results. For example, the top row in Fig. 11 indicates that a 50% variation in the yield level x_y results in variation for the equivalent stiffness term (Fig. 11a), and an even larger percentage variation for the equivalent viscous damping coefficient (Fig. 11b).

If only k_1 is randomized, the results indicate a relatively broad dispersion for the coefficients a_{10} (Fig. 11d) and a_{30} (Fig. 11f). However, the same percentage variation in the value of k_2 (see the third row from the top), results in the same mean value of the equivalent linear stiffness term a_{10}, but with very little dispersion with respect to its mean (Fig. 11g). The same comments apply to the other identified coefficients shown in Figs. 11h and 11i.

Notice, however, that as more system parameters are simultaneously randomized with a Gaussian distribution around their respective mean, the corresponding distributions of the dominant identified parameters a_{ij} resemble a PDF distribution with broader variance.

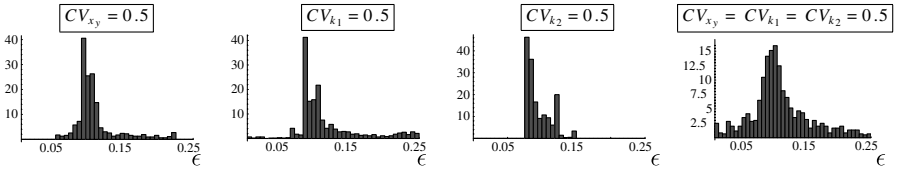

Fig. 10 PDF of normalized error ϵ for the four identification cases listed in Table 1.

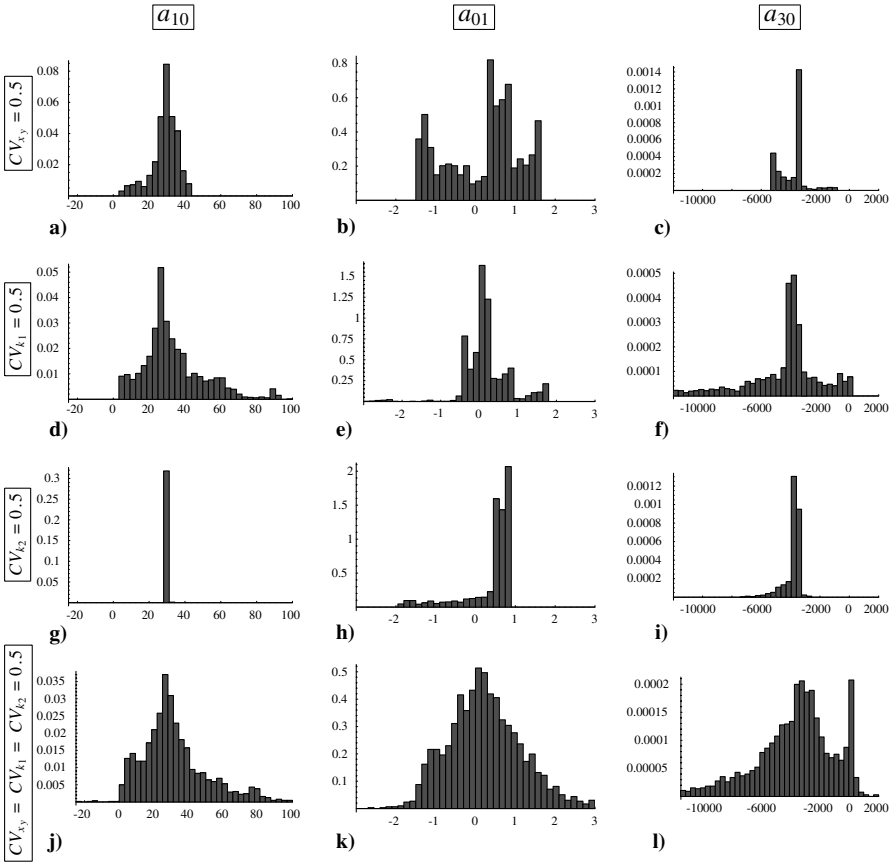

Fig. 11 Histograms of a_{ij} coefficients. The LHS column corresponds to a_{01}, the middle column to a_{01}, and the RHS column to a_{30}. In the top row, only x_y is randomized; in the second row from the top, only k_1 is randomized; in the third row, only k_2 is randomized; and in the bottom row, all three parameters x_y, k_1, and k_2 are simultaneously and independently randomized.

G. Relative Contribution of Dominant Restoring Force Terms

To appreciate the complex nonlinear dynamics involved in the hysteretic system under discussion, it is useful to obtain an estimate of the contribution of some of the dominant terms in the power-series coefficients to the overall restoring force. This is accomplished in Fig. 12 in which a summary of the contribution of four terms are shown: a_{10}, the equivalent linear stiffness term; a_{01}, the equivalent viscous damping term; a_{30}, the term that governs the contribution of cubic-stiffness force component; and a_{03}, the term that governs the contribution of the cubic-velocity force component. To enable convenient comparison of the relative contribution and significance of the various power-series terms, identical abscissa scales are used for all the plots shown in Fig. 12.

Each column of plots in Fig. 12 corresponds to a specific scenario of uncertain parameters: the LHS column corresponds to uncertainty in only x_y; the second column, to uncertainty in only k_1; the third column, to uncertainty in only k_2; and the fourth (RHS) column, to simultaneous uncertainty in x_y, k_1, and k_2.

In the actual hysteretic oscillator under discussion, the estimated restoring force magnitude $\hat{r}(t)$ at any time depends on very complex interactions between all the state variable combinations indicated in the power series shown in Eq. (3). The proper phasing of these various components in time generates the good estimates displayed in the preceding identification results. However, for the sake of simplifying the discussion so that first-order estimates of the contribution of various terms in the series of Eq. (3) are assessed, it is convenient to use the rms level as a gross indicator of the magnitude of a particular state variable, so that the individual contribution of a specific term in the doubly indexed series can be quantified.

With the preceding motivation in mind, the second row (from the top) of plots in Fig. 12 shows the contribution of the term $a_{10}x^1\dot{x}^0$ in each of the four simulation cases applied to the uncertain system. To obtain an estimate of the magnitude of this term contribution, the results displayed in the second row correspond to the distribution of the 2000 terms $\{a_{10}x^1_{\text{RMS}}\dot{x}^0_{\text{RMS}}\}_i$, with $i = 1, 2, \ldots, 2000$, for each simulation ensemble. Thus, the forces in this row can be thought of as the contribution of equivalent linear stiffness forces.

With the same idea in mind, the third row (from the top) of plots in Fig. 12 shows the contribution of the term $a_{01}x^0\dot{x}^1$ in each of the four simulation cases applied to the uncertain system. To obtain an estimate of the magnitude of this term contribution, the results displayed in the third row correspond to the distribution of the 2000 terms $\{a_{01}x^0_{\text{RMS}}\dot{x}^1_{\text{RMS}}\}_i$, with $i = 1, 2, \ldots, 2000$, for each simulation ensemble. Thus, the forces in this row can be thought of as the contribution of equivalent viscous damping forces.

Similarly, the fourth row (from the top) of plots in Fig. 12 shows the contribution of the term $a_{30}x^3\dot{x}^0$ in each of the four simulation cases applied to the uncertain system. Thus the forces in this row can be thought of as the contribution of the cubic-stiffness forces. Finally, the bottom row (from the top) of plots in Fig. 12 shows the contribution of the term $a_{03}x^0\dot{x}^3$ in each of the four simulation cases applied to the uncertain system. Thus, the forces in this row can be thought of as the contribution of the cubic-velocity forces.

It is worth pointing out again that the proper phase information is discarded in this estimate, and that there are several other significant nonlinear terms whose contribution is not displayed in Fig. 12, so as to keep the analysis of the results manageable.

III. Discussion

A. Modeling Issues

The statistical analysis results shown in Sec. II were based on an ensemble of 2000 items (test records). Had a much larger ensemble been generated, the resulting statistics (distributions, histograms, etc.) would have been smoother, but no material change would have occurred in the main conclusions drawn from the analysis of the results.

It is also worth pointing out that, although a specific generic nonlinear element was used as a representative nonlinear restoring

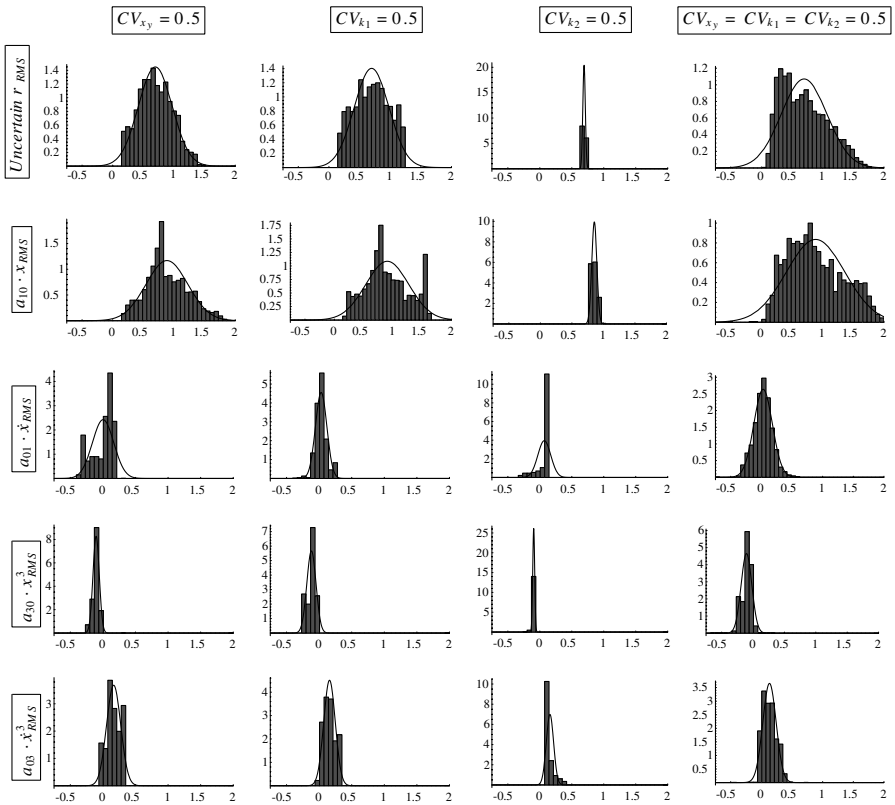

Fig. 12 Histograms of restoring force contributions of a_{ij} power-series terms to rms of restoring force. The first (top) row of plots corresponds to total rms of restoring force; the second row from the top, to contribution of coefficient a_{10}; the third row from the top, to a_{01}; the fourth row from the top, to a_{31}; and the bottom row, to a_{03}. The first (LHS) column of plots corresponds to uncertainty in only x_y; the second column, to uncertainty in only k_1; the third column, to uncertainty in only k_2; and the fourth (RHS) column, to simultaneous uncertainty in x_y, k_1, and k_2.

force, the complex nature of the illustrative hysteretic element used incorporates many of the challenging nonlinear phenomena typically encountered in complex multi-degree-of-freedom physical structures. Hence, the complex interaction of the excitation, with the propagation of various levels and combinations of uncertainties in specific parameters, and their subsequent projection onto the identified nonparametric model restoring force coefficients a_{ij}, have a much more broader relevance and applicability than to just the example system under discussion.

Although it is not surprising that, due to the highly nonlinear characteristics of the system under discussion, different features of the response (such as stiffnesslike, or dampinglike) are accentuated in different regimes (levels) of response, it is reassuring to see that, due to the nonparametric nature of the restoring force method, the dominant force components in the estimated restoring force do accurately evolve as the response features of the system change (e.g., from a complex, doubly curved nonlinear surface associated with softening/hardening characteristics, to one that is practically flat, as would be the case when the response is primarily due to equivalent linear effects). Notice that this is a crucial feature of the identification method under discussion, because the analyst need not worry about selecting a class of models (as would be needed in parametric identification approaches) to match the different regimes of motion that complex nonlinear systems may undergo, as their applied loads vary; the nonparametric approach by its nature does not assume any particular model form; it is a model-free representation.

It is also not surprising that the response of the uncertain hysteretic system (whose uncertain parameters have a Gaussian distribution) to a deterministic excitation should result in a dynamic response whose statistics do not possess a similar Gaussian distribution (see Fig. 5). Notice though that the non-Gaussian nature of the statistics of the identified restoring force coefficients, shown in Fig. 12, reflects the influence of the nonlinear system response as well as modeling errors, because the polynomial nature of the approximating function defining the estimated restoring force surface $\hat{r}(x, \dot{x})$ cannot exactly match the true nature of the actual hysteretic force (whose associated surface is more like a doughnut, and not just a single-valued, curved surface).

B. Statistics of Identified Coefficients

Table 5 provides a brief overview of the statistics of some major parameters associated with the motion and analysis of the hysteretic system under discussion when tested according to the four cases listed in Table 1. For each of the test cases, the table lists the standard deviation σ, the mean μ, and the coefficient of variation, defined as $CV = \sigma/\mu$ for each of the following parameters: the rms value of the system displacement, the rms value of the system restoring force, the dimensionless error ratio for the nonparametric identification procedure, as well as the values for five representative coefficients of the identified coefficients.

As previously discussed with reference to Fig. 6, the CV for case 3 (in which only k_2 was perturbed) has the smallest value of $\approx$0.02, and for case 4 (in which all parameters were randomized) it has the largest value of $\approx$0.30 among the four test cases. Similar comments apply for the statistics of r_{RMS}.

The influence of uncertainty in the actual system parameters on the corresponding uncertainty in the identified coefficients (as displayed in Fig. 11) can be conveniently discerned from analysis of the results shown in Table 5. The equivalent stiffness coefficient a_{10} is most sensitive to randomness in the hysteretic oscillator parameter k_1 (leading to a CV of $\approx$0.50) and least sensitive to perturbations in k_2 (leading to a CV of $\approx$0.02). On the other hand, the CV for the equivalent viscous damping term a_{01} reaches its largest value of $\approx$4.9 when the hysteretic oscillator yield level x_y is randomized and assumes a much reduced value of $\approx$1.5 when k_2 is randomized. In either case, it is worth noting that due to its reduced influence on the total restoring force, there is substantially more uncertainty reflected in the dominant dampinglike coefficients as compared with the stiffnesslike coefficients. Considering case 4, when all system parameters were simultaneously randomized, the CV for the stiffness coefficient a_{10} is $\approx$0.6, whereas the corresponding CV for the damping coefficient a_{01} is $\approx$3.6, an increase by about a factor of six.

C. Prediction of Stochastic Dynamic System Response

The long-range aim of this study is to develop predictive models that can provide their predictions with a probabilistic scatter commensurate with experimental evidence. This entails, when relying on the nonparametric models described previously to carry out the predictions, the characterization of the coefficients in the models as stochastic quantities. In addition to representing the nonparametric coefficients in orthogonal expansions, all quantities of interest (such as peak values, excursion times, etc.) can be represented in a similar manner, resulting in a uniform characterization of the behavior of the nonlinear element. An overview of the planned approach follows.

In the context of the present study, a typical stochastic quantity $C(\theta)$ can be represented as

$$C(\theta) = \sum_{p=0}^{P_1} C_p \psi_p(\theta) \tag{4}$$

These are typically orthogonal polynomials in some standard random variable (Gaussian, uniform, etc.), the exact distribution of which depends on the particular data at hand. Although expansions with respect to any orthogonal polynomial will converge in mean square, the rate of convergence will depend on how adapted the particular choice of polynomials is to the problem.

The coefficients C_p in the preceding equation can be computed as generalized Fourier coefficients by projecting the equation on $\psi_p(\theta)$, resulting in

$$C_p = \frac{\langle C(\theta)\psi_p(\theta)\rangle}{\langle \psi_p^2 \rangle} \tag{5}$$

Thus, starting with observations of $C(\theta)$, the preceding procedure permits the evaluation of the associated coefficients C_p (Sakamoto and Ghanem [8,9]). A standard such procedure relies on orthogonal projections, resulting in a system of deterministic equations to be solved for the unknown coefficients.

Once a representation of the coefficients has been computed, it can be substituted into the governing equation. A similar expansion for

Table 5 Statistical analysis of identification results

	Case 1			Case 2			Case 3			Case 4		
Parameter	σ	μ	CV	σ	μ	CV	σ	μ	CV	σ	μ	CV
x_{RMS}	0.005	0.030	0.154	0.007	0.029	0.239	0.001	0.029	0.024	0.009	0.030	0.289
r_{RMS}	0.275	0.696	0.396	0.284	0.697	0.408	0.020	0.692	0.028	0.373	0.697	0.535
ϵ	0.036	0.112	0.319	0.047	0.117	0.400	0.016	0.095	0.170	0.064	0.117	0.542
a_{00}	0.045	0.041	1.099	0.068	0.064	1.067	0.047	0.030	1.538	0.066	0.041	1.605
a_{10}	7.387	28.541	0.259	17.381	33.534	0.518	0.704	29.297	0.024	18.896	31.528	0.599
a_{01}	0.924	0.189	4.898	0.632	0.184	3.443	0.621	0.405	1.533	0.998	0.276	3.615
a_{30}	1087	−3715	−0.293	5996	−6311	−0.950	559	−3857	−0.145	5041	−4892	−1.030
a_{03}	14.78	27.36	0.54	25.47	40.31	0.632	16.01	34.7	0.46	26.31	28.26	0.931

the solution is then sought of the form

$$x(t,\theta) = \sum_{p=0}^{P_2} x_p(t)\psi_p(\theta) \tag{6}$$

The coefficients in the representation can be obtained in one of two ways. The first consists of evaluating them as generalized Fourier coefficients in the form

$$x_p(t) = \frac{\langle x(t,\theta)\psi_p(\theta)\rangle}{\langle \psi_p^2\rangle} \tag{7}$$

The second procedure consists of substituting this representation in the governing equation of motion and forcing both sides of the equation to be equal in the weak sense [i.e., projecting both sides of the equation on $\psi_p(\theta)$]. This yields a system of $(P_2 + 1)$ equations to solve for the unknown coefficients $x_p(t)$.

This stochastic prediction formalism generalizes the nonparametric reduced-order models used for representing the restoring force, previously detailed in this paper. It extends that approach to the stochastic component of the problem, permitting a robust representation of uncertainty. Further details concerning this approach, and an illustrative example application to an uncertain linear single-degree-of-freedom system, are available in the work of Ghanem et al. [27].

IV. Conclusion

A single-degree-of-freedom system with bilinear hysteretic characteristics is used to investigate the propagation of uncertainties in the dominant parameters that control the idealized restoring force associated with such a system: the yield level, the stiffness in the elastic range, and the stiffness in the yielded range. Random variations with a specific probability distribution are introduced in the nominal (mean) value of each of the dominant parameters. The effects of uncertainties are evaluated under four scenarios: 1) uncertainties only in the yield level, 2) uncertainties only in the elastic range stiffness, 3) uncertainties only in the yielded range stiffness, and 4) simultaneous (and independent) uncertainties in all the dominant parameters.

Monte Carlo simulation approaches are used to generate a large, statistically significant ensemble of time history records that are subsequently used to determine the distribution of the corresponding transient response and to establish the probabilistic bounds on the response time history. For each member of the four ensemble groups, a nonparametric identification approach based on the restoring force method is used to determine, through a least-squares fit, the power-series coefficients that define an equivalent, approximating surface that characterizes the system behavior. The statistics of the identified coefficients are determined and shown to provide a powerful tool for quantifying the level of uncertainty in the nonlinear system, as well as providing a means for interpreting the significant features of the underlying complex nonlinear behavior.

Furthermore, it is shown that the general methodology presented for representing and propagating the effects of uncertainties in complex nonlinear systems through the use of model-free representation allows the estimation through analytical procedures of the uncertain system's response bounds when excited by a different dynamic load than the one used to identify it.

Acknowledgments

This study was supported in part by grants from the U.S. Air Force Office of Scientific Research and the National Science Foundation. The editorial assistance of E. Kallinikidou in the preparation of the manuscript is appreciated.

References

[1] Ghanem, R., "Ingredients for a General Purpose Stochastic Finite Elements Formulation," *Computer Methods in Applied Mechanics and Engineering*, Vol. 168, Nos. 1–4, 1999, pp. 19–34.

[2] Ibrahim, R. A., "Structural Dynamics with Parametric Uncertainties," *Applied Mechanics Reviews*, Vol. 40, No. 3, Mar. 1987, pp. 309–328.

[3] Ibrahim, R. A., and Pettit, C. L., "Uncertainties and Dynamic Problems of Bolted Joints and Other Fasteners," *Journal of Sound and Vibration*, Vol. 279, No. 3–5, 2003, pp. 857–936.

[4] Lin, Y. K., and Cai, G. Q., *Probabilistic Structural Dynamics, Advanced Theory and Applications*, McGraw–Hill, New York, 1995.

[5] Pettit, C. L., "Uncertainty Quantification for Airframes: Current Status, Needs, and Suggested Directions," Society of Automotive Engineers, Paper 03M-123, 2002.

[6] Pellissetti, M., and Ghanem, R., "A Method for the Validation of Predictive Computations Using a Stochastic Approach," *Journal of Offshore Mechanics and Arctic Engineering*, Vol. 126, No. 3, 2004, pp. 227–234.

[7] Sakamoto, S., and Ghanem, R., "Simulation of Multi-Dimensional Non-Gaussian Non-Stationary Random Fields," *Probabilistic Engineering Mechanics*, Vol. 17, No. 2, April 2002, pp. 167–176.

[8] Sakamoto, S., and Ghanem, R., "Polynomial Chaos Decomposition for the Simulation of Non-Gaussian Non-Stationary Stochastic Processes," *Journal of Engineering Mechanics*, Vol. 128, No. 2, Feb. 2002, pp. 190–201.

[9] Soize, C., and Ghanem, R., "Physical Systems with Random Uncertainties: Chaos Representations with Arbitrary Probability Measure," *Journal of Scientific Computing*, Vol. 26, No. 2, 2005, pp. 395–410.

[10] Spanos, P., and Ghanem, R., "Stochastic Finite Element Expansion for Random Media," *Journal of Engineering Mechanics*, Vol. 115, No. 5, May 1989, pp. 1035–1053.

[11] Housner, G. W., Bergman, L. A., Caughey, T. K., Chassiakos, A. G., Claus, R. O., Masri, S. F., Skelton, R. E., Soong, T. T., Spencer, B. F., and Yao, J. T. P., "Structural Control: Past, Present and Future," *Journal of Engineering Mechanics*, Vol. 123, No. 9, Sept. 1997, pp. 897–971.

[12] Wen, Y. K., "Method for Random Vibration of Hysteretic Systems," *Journal of Engineering Mechanics*, Vol. 102, No. EM2, 1976, pp. 249–263.

[13] Androniku, A. M., Bekey, G. A., and Masri, S. F., "Identification of Nonlinear Hysteretic Systems Using Random Search," *Proceedings of the 6th IFAC Symposium on Identification and System Parameter Estimation*, International Federation of Automatic Control, Washington, D.C., 1982, pp. 1–8.

[14] Worden, K., "Parametric and Nonparametric Identification of Nonlinearity in Structural Dynamics," Ph.D. Dissertation, Dept. of Mechanical Engineering, Heriot–Watt Univ., Edinburgh, Scotland, U. K., 1989.

[15] Chassiakos, A. G., Masri, S. F., Smyth, A. W., and Caughey, T. K., "On-Line Identification of Hysteretic Systems," *Journal of Applied Mechanics*, Vol. 65, March 1998, pp. 194–203.

[16] Banks, H. T., Smith, R. C., and Wang, Y., *Smart Material Structures: Modeling, Estimation and Control*, Masson, Paris, and Wiley, Chichester, England, U.K., 1996.

[17] Banks, H. T., Kurdila, A. J., and Webb, G., "Identification of Hysteretic Control Influence Operators Representing Smart Actuators Part 1: Formulation," *Mathematical Problems in Engineering*, Vol. 3, 1997, pp. 287–328.

[18] Banks, H. T., Kurdila, A. J., and Webb, G., "Identification of Hysteretic Control Influence Operators Representing Smart Actuators Part 2: Convergent Approximations," *Journal of Intelligent Material Systems and Structures*, Vol. 8, No. 6, 1997,pp. 536–550.

[19] Smyth, A. W., Masri, S. F., Chassiakos, A. G., and Caughey, T. K., "On-Line Parametric Identification of MDOF Nonlinear Hysteretic Systems," *Journal of Engineering Mechanics*, Vol. 125, No. 2, 1999.

[20] Smyth, A. W., Masri, S. F., Kosmatopoulos, E. B., Chassiakos, A. G., and Caughey, T. K., "Development Of Adaptive Modeling Techniques for Non-Linear Hysteretic Systems," *International Journal of Nonlinear Mechanics*, Vol. 37, 2002, pp. 1435–1451.

[21] Masri, S. F., and Caughey, T. K., "A Nonparametric Identification Technique for Nonlinear Dynamic Problems," *Journal of Applied Mechanics*, Vol. 46, June 1979, pp. 433–447.

[22] Masri, S. F., Caffrey, J. P., Caughey, T. K., Smyth, A. W., and Chassiakos, A. G., "A General Data-Based Approach for Developing Reduced-Order Models of Nonlinear MDOF Systems," *Nonlinear Dynamics*, Vol. 39, Jan. 2005, pp. 95–112.

[23] Anderson, J. C., Masri, S. F., Miller, R. K., Sassi, H., and Caughey, T. K., "Identification of a Nonlinear Building Model from Response Measurements Under Earthquake Excitation," *Proceedings of the Eighth World Conference on Earthquake Engineering*, International Association for Earthquake Engineering (IAEE), San Francisco, 1984, Vol. 6., pp. 95–102.

[24] Masri, S. F., Miller, R. K., Traina, M. I., and Caughey, T. K., "Development of Bearing Friction Models from Experimental Measurements," *Journal of Sound and Vibration*, Vol. 148, No. 3, August 1991, pp. 455–475.

[25] Worden, K., and Tomlinson, G. R., *Nonlinearity in Structural Dynamics: Detection, Identification and Modelling*, Inst. of Physics, London, 2001.

[26] Masri, S. F., Caffrey, J. P., Caughey, T. K., Smyth, A. W., and Chassiakos, A. G., "Identification of the State Equation in Complex Nonlinear Systems," *International Journal of Non-Linear Mechanics*, Vol. 39, 2004, pp. 1111–1127.

[27] Ghanem, R., Masri, S. F., Pellissetti, M., and Wolfe, R., "Identification and Prediction of Stochastic Dynamical Systems in a Polynomial Chaos Basis," *Computer Methods in Applied Mechanics and Engineering*, Vol. 194, No. 12–16, 2005, pp. 1641–1654.

A. Berman
Associate Editor